RESEARCH ARTICLE | JUNE 02 2022

Experimental study of electromagnetic wave scattering from a gyrotropic gaseous plasma column ⊘

Luc S. Houriez ⓘ ; Hossein Mehrpour Bernety ⓘ ; Jesse A. Rodríguez ⓘ ; Benjamin Wang;
Mark A. Cappelli ✉ ⓘ

Check for updates
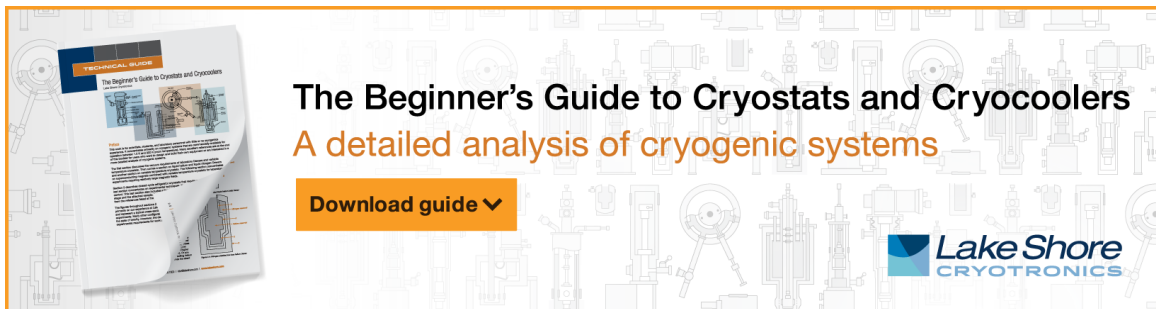
🌐 View Online

↪ Export Citation

CrossMark

Experimental study of electromagnetic wave scattering from a gyrotropic gaseous plasma column

View Online   Export Citation   CrossMark

Luc S. Houriez, (iD) Hossein Mehrpour Bernety, (iD) Jesse A. Rodríguez, (iD) Benjamin Wang, and Mark A. Cappelli[a] (iD)

AFFILIATIONS

Department of Mechanical Engineering, Stanford University, Stanford, California 94305, USA

[a]Author to whom correspondence should be addressed: cap@stanford.edu

ABSTRACT

We experimentally demonstrate the controlled scattering of incident transverse-electric electromagnetic waves from a gyrotropic magnetized plasma cylindrical discharge. Scattered electromagnetic waves can bend left and right by changing the external magnetic field of a plasma rod. Measured scattered wavefronts are in good agreement with electromagnetic simulations. A gyrotropic response is observed for incident wave frequencies ranging from 3.5 to 5.6 GHz for conditions corresponding to a ratio of cyclotron frequency to plasma frequency, $\omega_{ce}/\omega_p \approx 0.16$. The observation of a gyrotropic response from cylindrical plasma discharges paves the way for their use as building blocks for future devices such as magnetized plasma photonic crystals, topological insulators, plasma metamaterials, non-reciprocal waveguide structures, and other devices, which require a tunable gyrotropic response from centimeter to meter-scale materials with application-specific geometry.

Published under an exclusive license by AIP Publishing. https://doi.org/10.1063/5.0095038

The control of electromagnetic waves has long been the interest of researchers in physics and engineering. Alternative methods of redirecting, filtering, modulating, and attenuating waves have led to various applications in wireless sensing and communication. In recent years, the development of engineered metamaterials has led to properties such as negative refraction and near-zero permittivity that are not attainable in natural or previously synthesized materials. Negative refraction enables cloaking[1–3] as well as the ability to focus waves to below the diffraction limit.[4]

The research on engineered photonic and plasmonic structures, some of which behave as optical analogs to topological electrical insulators,[5–7] have led to more exotic electromagnetic wave control. Most of these previous studies have been focused on the use of metallic and dielectric materials as the constituent building blocks, althoughgases and liquids have recently been used for constructing the metamaterial or photonic domains.

One interesting medium that has only recently been explored for incorporation into such structures is a gaseous plasma. Gaseous plasmas possess unique features not present in other material phases such as low collisional damping and continuously variable physical properties that can be tuned in time and space. Often modeled to have a Drude dielectric response where the tunable parameter is plasma density, the relative permittivity of plasma ε_p can be adjusted to achieve metallic ($\varepsilon_p < 0$) or dielectric ($0 < \varepsilon_p < 1$) behavior with a temporal response limited by rates of plasma recombination or ionization.

A magnetized plasma has an anisotropic permittivity that results in a gyrotropic response. As a result, it is a topologically non-trivial bulk material that can possess chiral, unidirectional interfacial edge states that are immune to scattering.[7–9] This behavior leads to non-reciprocity, enabling potentially reconfigurable or tunable one-way waveguides that may be of interest in various applications.

However, experimental plasmas exhibit many non-ideal factors that represent a disconnect between what is experimentally plausible and the exciting theoretical results previously demonstrated for gyrotropic materials. As such, producing a bulk, uniform magnetized plasma medium with geometry tailored to specific applications is not feasible in practice. To combat this, devices composed of smaller gyrotropic elements, such as the cylindrical plasma discharges in this study, can be designed to exhibit the same physics as a larger bulk gyrotropic medium. Before using such smaller components, however, it is important that their gyrotropic response is confirmed and well-characterized.

Leveraging the understanding gathered from past simulations and theoretical studies that describe the scattering from a gyrotropic

plasma column,[10–13] this paper demonstrates a low-pressure magnetized plasma discharge with an electromagnetic gyrotropic response. Characterization of this phenomenon allows it to be utilized as an experimentally viable component for photonic devices such as magnetized plasma metamaterials and photonic crystals, non-reciprocal waveguide structures, and other devices that require a tunable gyrotropic response.

An experimental platform is designed and fabricated to study the scattered wave from a magnetized plasma rod. Figure 1 shows the experimental setup, which consists of a broadband microwave horn antenna (A INFO LB-20180 2—18 GHz) that is used to send incident transverse-electric polarized (TE) electromagnetic waves from 3 to 8 GHz in frequency along the x-axis defined in Fig. 1(b). In this study, we define the TE polarization such that the electric field of the source is perpendicular to the plasma rod. The gaseous plasma discharge is positioned in the path of the wave and placed in the center of a Helmholtz coil setup to allow for axial magnetization of the plasma discharge. The scattered wave from the plasma rod is measured by the open-source electromagnetic field robot OpenEM.[14] The robot consists of two orthogonal stepper motors positioned 6 cm away from the rod, allowing it to map a 15×30 cm^2 area with a 0.75 cm step size. A computer controls the linear stages using OpenEM Labview software, and the amplitude and the phase of the wave are measured at each mapping grid point via a vector network analyzer (HP 8722D). θ is defined as the angle at the rod's center between each point of the mapped area and the x-axis shown in Fig. 1(b).

The plasma rod is a custom-fabricated discharge source consisting of a 15 mm diameter quartz tube with an inner wall thickness of 1 mm and a length of 290 mm, filled to approximately 250 Pa with argon and added mercury, the vapor pressure of which is determined by the operating temperature. The gas temperature during nominal operation is approximately 330 K, resulting in a mercury vapor partial pressure of about 3.5 Pa. The discharge is driven by an alternating-current (AC) ballast at 33.1 kHz frequency with 144 V peak-to-peak voltage and 298 mA root mean square (RMS) discharge current at the nominal operating condition. These types of plasma discharge tubes have been used in our past studies as non-magnetized inclusions in dielectric photonic crystals[15,16] and as the basic building block for 2D

and 3D non-magnetized plasma photonic crystals.[17,18] The plasma density is tuned by using a variable AC transformer to vary the AC voltage delivered to the ballast, resulting in a typical achievable plasma frequency range of about 2–9 GHz. These plasma frequencies, as well as other plasma properties such as mean electron energy and electron momentum scattering frequency, can be estimated from discharge operating conditions such as the RMS voltage and current, fill pressure, and discharge geometry (area and length of the positive column), via BOLSIG+,[15,19] which is an online tool that solves the zero-dimensional Boltzmann equation for the electron energy distribution function in the local field approximation. From an estimate of the local reduced electric field, BOLSIG+ returns the mean electron energy, electron mobility, and electron momentum collision frequency. For the conditions in which the electromagnetic scattering is studied in this paper, the BOLSIG+ suggests that the plasma and collision frequencies are approximately 9 and 2.3 GHz, respectively, and the electron temperature is approximately 1.7 eV, assuming a current-carrying plasma diameter of 13 mm.[20]

The Helmholtz arrangement for generating the external magnetic field consists of two water-cooled coils driven by a DC power supply (10 A, 100 V). The setup provides a quasi-uniform 47.5 mT magnetic field for magnetically biasing the plasma placed at the center of the coils. The upper and lower coils are conduction cooled using lines that circulate water at 2.5 °C to eight aluminum cooling pods in contact with the coils. A block diagram depicting functional elements of the entire setup is shown in Fig. 2.

We investigate the scattered field for two different plasma configurations: magnetized with an upwards oriented magnetic field (B+) and a downwards oriented magnetic field (B−). Experimental results are complemented by corresponding electromagnetic simulations to better understand the dynamics of the scattering fields from the magnetized plasma column. Figure 3(a) plots the scattered field's normalized Poynting vector S/S_{max} obtained using the frequency-domain solver from Computer Simulation Technology (CST) Microwave Studio 2022.[21] The plasma rod is 3D modeled as a smaller gyrotropic plasma core (4.5 mm in radius) separated from a 1 mm thick quartz envelope (inner radius of 6.5 mm) by a thin, 2 mm non-ionized gap
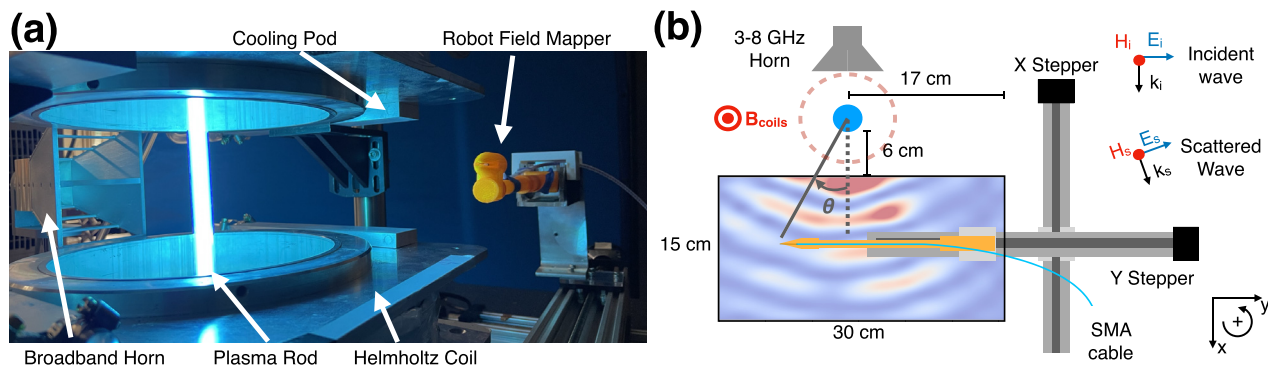

FIG. 1. (a) Laboratory photograph of the experimental setup showing the EM field-mapping robot scanning the scattered field from an active plasma rod placed within Helmholtz coils. The coils are conduction water-cooled to allow for long-term operation. (b) Top view schematic of the experimental setup depicting the robot, the mapped area (outlined in solid black), and relevant distances. The field-mapping robot uses two linear translation stages to map a rectangular area (15×30 cm^2 area with a 0.75 cm step size) on the $z = 0$ plane bisecting the two Helmholtz coils.
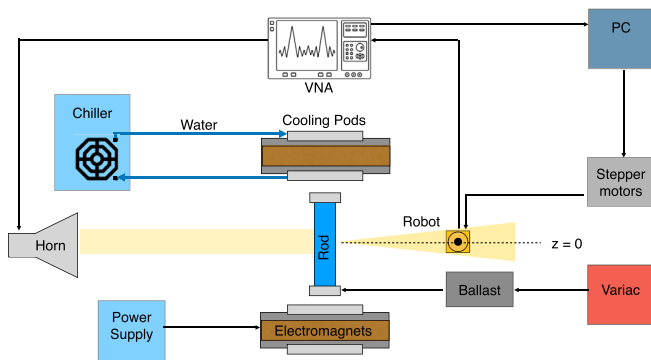
FIG. 2. Block diagram depicting the functional elements of the entire experimental setup. All probe measurements are taken on the z = 0 plane.

(with vacuum permittivity) to account for the non-uniform density profile in the bulb. This three layer model is a simple representation of the actual distribution of plasma density within a discharge tube,[22] and the results are in acceptable agreement with experiments involving plasma photonic crystals.[17,18] In the simulations, we use periodic
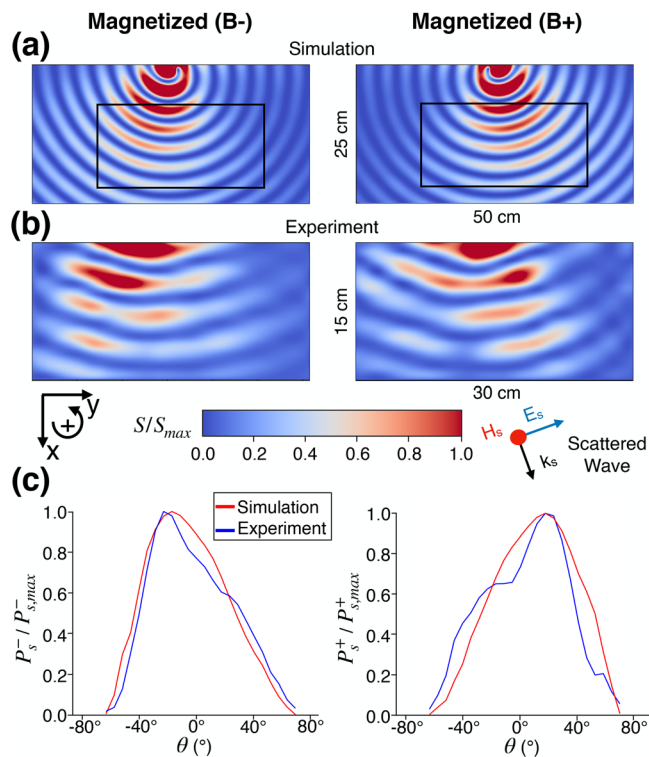

FIG. 3. Normalized Poynting vector of a 4.42 GHz scattered wave from a magnetized plasma rod: (a) simulated using CST and (b) experimentally measured in the 15 × 30 cm² region represented by the black rectangle. (c) Normalized scattered power derived from experiments and simulations in the black rectangle region at 4.42 GHz.

boundary conditions along the z-axis to mimic an infinitely long plasma column. The computed scattered fields are also in the z = 0 plane consistent with the experimental measurements. The plasma frequency, electron momentum collision frequency, and cyclotron frequency are $\omega_p = 5.28 \times 10^{10}$ rad/s, $\nu_c = 1.34$ GHz, and $\omega_{ce} = 8.4 \times 10^9$ rad/s, respectively. The values for ω_p and ν_c used to obtain optimal agreement between measured and computed scattering, while slightly different than those estimated from previous non-magnetized studies, are consistent with estimates derived from the BOLSIG+ simulations.

The plasma's relative anisotropic permittivity $(\bar{\bar{\varepsilon}}_p)$, which is responsible for its gyrotropic scattering, assuming a time dependence of the form $e^{+j\omega t}$, is given by

where

$$\bar{\bar{\varepsilon}}_p = \begin{bmatrix} \varepsilon_t & j\varepsilon_g & 0 \\ -j\varepsilon_g & \varepsilon_t & 0 \\ 0 & 0 & \varepsilon_z \end{bmatrix}, \tag{1a}$$

$$\varepsilon_t = 1 - \frac{\omega_p^2 (\omega - j\nu_c)}{\omega \left[(\omega - j\nu_c)^2 - \omega_{ce}^2 \right]}, \tag{1b}$$

$$\varepsilon_g = -\frac{\omega_p^2 \omega_{ce}}{\omega \left[(\omega - j\nu_c)^2 - \omega_{ce}^2 \right]}, \tag{1c}$$

$$\varepsilon_z = 1 - \frac{\omega_p^2}{\omega(\omega - j\nu_c)}. \tag{1d}$$

The permittivity tensor, non-symmetric due to the applied magnetic bias, defines the interaction of the electromagnetic wave with electrons within the plasma. Governing the off-diagonal terms, ε_g characterizes the strength of the gyrotropy of the magnetoplasma. In a non-magnetized plasma, permittivity is isotropic and the radiated wave from the plasma rod is oriented in the direction of propagation of the incident wave. As a result of the interaction with a gyrotropic plasma rod, the radiated field from the excited plasma is rotated.

Figure 3(b) presents the normalized Poynting vector S/S_{max} of the scattered electromagnetic field experimentally measured at 4.42 GHz in the area delimited by the black box on the simulation results. Experimentally, a scattered wave is obtained by performing two wavefronts scans. For the first scan, the plasma discharge is removed, and the incident wave emitted by the horn is mapped out. For the second scan, the plasma discharge is inserted, the magnetic coils are activated, and the incident and scattered waves are collected by the robot with amplitude and phase recorded at the exact same locations as for the first scan. The scattered wave is calculated by subtracting these two scans. We see that the electromagnetic simulations and experimental measurements are in good agreement. There is a clear asymmetry in the scattering induced by the magnetized plasma, a confirmation of the active gyrotropic response. For an upwards oriented (B+) field, the scattered field is gyrotropically bent to the left of the x-axis along which the incident wave is propagating. For a downwards oriented (B−) field, the scattered field is gyrotropically bent to the right of the x-axis. This experimentally demonstrates the ability to bend electromagnetic waves using a magnetized plasma rod by changing the direction of the axially applied magnetic field on the plasma.

In the black boxed region of Fig. 3(a), the scattered power P_s is computed at every angle θ of the experimental and simulated wavefronts by integrating the Poynting vector along a given θ. Figure 3(c) presents the scattered power in the (B−) and the (B+) configurations, respectively, denoted by P_s^- and P_s^+. Good quantitative agreement is obtained between simulated and experimental results, and peak scattered power is notably reached at equal angles.

Figure 4 shows the difference, $\Delta P = P_s^- - P_s^+$, of experimentally obtained scattered powers at every angle θ between the (B+) and (B−) configurations over the 3.50–5.65 GHz range, normalized by the maximum scattered power difference, ΔP_{max}, detected over this range. In the (B−) configuration, scattering into negative angles is favored, and in the (B+) configuration, scattering into positive angles is favored. The peak scattered power is approximately situated between 20° and 40° over this range of frequencies. As expected from previous theoretical studies of a collisionless magnetized plasma,[10] some frequencies seem to display stronger degrees of gyrotropic response. In our experimental study, such a frequency band is located around 5.15 GHz. Furthermore, we expect the maximum scattered power's angle to change with variations in the magnitude of the external magnetic field.[10] For example, CST simulations at 4.42 GHz suggest that doubling the external magnetic field keeping all other parameters constant could double this angle derived from the black-boxed region in Fig. 3(a).

The fact that this magnetically biased plasma is indeed gyrotropic is not unexpected as the anticipated electron Hall parameter with collisionality estimated from these scattering measurements suggests that for these discharges, $\omega_{ce}/\nu_c \approx 6$, consistent for conditions of modestly magnetized electrons. Furthermore, assuming an electron temperature of $T_e \approx 1.7$ eV as estimated from the BOLSIG+ simulations (mean electron speed, $c_e \approx \times 10^6$ m/s), the electron gyroradius, $r_g \approx \times 10^{-4}$ m, is much smaller than the plasma discharge diameter, and so the plasma is not expected to be significantly demagnetized by electron collisions with the quartz wall.
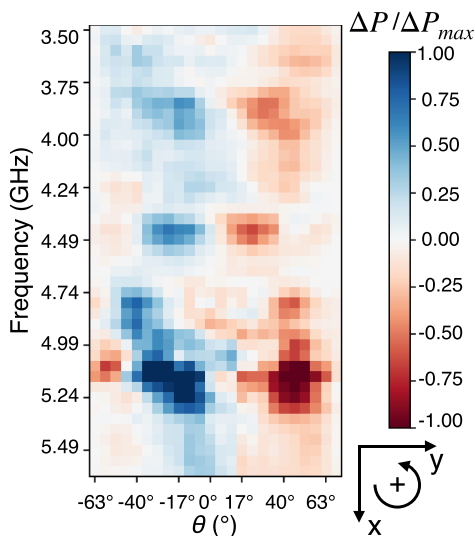

FIG. 4. Normalized experimental scattered power difference between the (B−) and the (B+) configurations as a function of the angle and frequency.

In conclusion, we demonstrated a magnetically biased low-pressure plasma discharge with substantial gyrotropic response despite non-ideal experimental factors such as plasma collisionality. This response is detected in the 3.5–5.6 GHz frequency regime by measuring the rotation in the forward-scattered wave phase fronts. Our experimental investigation is in good quantitative and qualitative agreement with simulations. As such, this study paves the way toward the use of these plasma elements as building blocks for complex devices such as magnetized plasma photonic crystals, metamaterials, topological insulators, and non-reciprocal waveguides.

AUTHOR DECLARATIONS
Conflict of Interest

The authors have no conflicts to disclose.

Author Contributions

Luc S. Houriez: Conceptualization (equal); Data curation (lead); Formal analysis (lead); Funding acquisition (equal); Investigation (lead); Methodology (lead); Software (lead); Supervision (equal); Validation (equal); Visualization (lead); Writing – original draft (equal); Writing – review & editing (equal). **Hossein Mehrpour Bernety:** Conceptualization (equal); Data curation (supporting); Formal analysis (supporting); Investigation (supporting); Methodology (supporting); Software (equal); Validation (equal); Visualization (supporting); Writing – original draft (equal); Writing – review & editing (equal). **Jesse A. Rodríguez:** Conceptualization (supporting); Data curation (supporting); Formal analysis (supporting); Investigation (supporting); Methodology (equal); Software (supporting); Validation (supporting); Visualization (supporting); Writing – original draft (supporting); Writing – review & editing (supporting). **Benjamin Wang:** Conceptualization (supporting); Data curation (supporting); Formal analysis (supporting); Investigation (supporting); Methodology (equal); Software (supporting); Visualization (supporting); Writing – original draft (supporting); Writing – review & editing (supporting). **Mark A. Cappelli:** Conceptualization (equal); Formal analysis (equal); Funding acquisition (lead); Methodology (supporting); Project administration (lead); Resources (lead); Supervision (lead); Writing – original draft (equal); Writing – review & editing (equal).

DATA AVAILABILITY

The data that support the findings of this study are available from the corresponding author upon reasonable request.

REFERENCES

[1] J. B. Pendry, D. Schurig, and D. R. Smith, "Controlling electromagnetic fields," Science **312**, 1780–1782 (2006).

[2]A. Alù and N. Engheta, "Achieving transparency with plasmonic and metamaterial coatings," Phys. Rev. E **72**, 016623 (2005).

[3]G. W. Milton and N.-A. P. Nicorovici, "On the cloaking effects associated with anomalous localized resonance," Proc. R. Soc. A **462**, 3027–3059 (2006).

[4]R. Chatterjee, N. C. Panoiu, K. Liu, Z. Dios, M. B. Yu, M. T. Doan, L. J. Kaufman, R. M. Osgood, and C. W. Wong, "Achieving subdiffraction imaging through bound surface states in negative refraction photonic crystals in the near-infrared range," Phys. Rev. Lett. **100**, 187401 (2008).

[5]Z. Wang, Y. Chong, J. D. Joannopoulos, and M. Soljačić, "Observation of unidirectional backscattering-immune topological electromagnetic states," Nature **461**, 772–775 (2009).

[6]L. Lu, J. D. Joannopoulos, and M. Soljačić, "Topological photonics," Nat. Photonics **8**, 821–829 (2014).

[7]S. Pakniyat, A. M. Holmes, G. W. Hanson, S. A. H. Gangaraj, M. Antezza, M. G. Silveirinha, S. Jam, and F. Monticone, "Non-reciprocal, robust surface plasmon polaritons on gyrotropic interfaces," IEEE Trans. Antennas Propag. **68**, 3718–3729 (2020).

[8]B. Yang, M. Lawrence, W. Gao, Q. Guo, and S. Zhang, "One-way helical electromagnetic wave propagation supported by magnetized plasma," Sci. Rep. **6**, 21461 (2016).

[9]J. B. Parker, J. Marston, S. M. Tobias, and Z. Zhu, "Topological gaseous plasmon polariton in realistic plasma," Phys. Rev. Lett. **124**, 195001 (2020).

[10]C. Valagiannopoulos, S. A. H. Gangaraj, and F. Monticone, "Zeeman gyrotropic scatterers: Resonance splitting, anomalous scattering, and embedded eigenstates," Nanomater. Nanotechnol. **8**, 184798041880808 (2018).

[11]V. A. Es'kin, A. V. Ivoninsky, and A. V. Kudrin, "Scattering of an obliquely incident plane electromagnetic wave by a magnetized plasma column: Energy flow patterns at plasmon resonances," Prog. Electromagn. Res. B **63**, 173–186 (2015).

[12]V. A. Es'kin, A. V. Ivoninsky, and A. V. Kudrin, "The energy flow behavior during the resonance scattering of a plane electromagnetic wave by a magnetized plasma column," in *The 8th European Conference on Antennas and Propagation (EuCAP 2014)* (IEEE, 2014) pp. 2754–2757.

[13]A. V. Kudrin, A. V. Ivoninsky, and V. A. Es'kin, "Radiation characteristics of filamentary sources in the presence of periodically spaced nonreciprocal cylindrical scatterers," in *12th European Conference on Antennas and Propagation (EuCAP 2018)* (IEEE, 2018), pp. 1–3.

[14]B. Wang, R. Sud, M. Leung, M. Yang, J. A. Rodriguez, R. Lee, and M. Cappelli, "OpenEM—Electromagnetic field mapping robot for microwave and RF measurements," Hardware X **5**, e00062 (2019).

[15]B. Wang and M. Cappelli, "A tunable microwave plasma photonic crystal filter," Appl. Phys. Lett. **107**, 171107 (2015).

[16]B. Wang, J. A. Rodríguez, O. Miller, and M. A. Cappelli, "Reconfigurable plasma-dielectric hybrid photonic crystal as a platform for electromagnetic wave manipulation and computing," Phys. Plasmas **28**, 043502 (2021).

[17]B. Wang and M. Cappelli, "A plasma photonic crystal bandgap device," Appl. Phys. Lett. **108**, 161101 (2016).

[18]B. Wang, J. A. Rodriguez, and M. Cappelli, "3D woodpile structure tunable plasma photonic crystal," Plasma Sources Sci. Technol. **28**, 02LT01 (2019).

[19]G. J. M. Hagelaar and L. C. Pitchford, "Solving the Boltzmann equation to obtain electron transport coefficients and rate coefficients for fluid models," Plasma Sources Sci. Technol. **14**, 722–733 (2005).

[20]B. Wang, "A theoretical and experimental investigation of plasma photonic crystals and devices," Doctoral dissertation (Stanford University, 2022).

[21]See www.cst.com for "Computer Simulation Technology, Microwave Studio."

[22]Y. Liang, Z. Liu, L. Lin, J. Peng, R. Liu, and Q. Lin, "Transmission characteristics of electromagnetic waves in 2D tunable plasma photonic crystals," Appl. Opt. **60**, 2510 (2021).

12 August 2023 04:48:26